

## The characterization of InN growth under high-pressure CVD conditions

N. Dietz<sup>\*1</sup>, M. Alevli<sup>1</sup>, V. Woods<sup>1</sup>, M. Strassburg<sup>1</sup>, H. Kang<sup>2</sup>, and I. T. Ferguson<sup>2</sup>

<sup>1</sup> Department of Physics and Astronomy, Georgia State University, Atlanta, GA 30303, USA

<sup>2</sup> School of Electrical & Computer Engineering, Georgia Institute of Technology, Atlanta, GA 30332, USA

Received 25 July 2005, revised 23 August 2005, accepted 24 August 2005

Published online 20 October 2005

PACS 78.20.Ci, 78.30.Fs, 81.05.Ea, 81.15.Kk

Gaining insight into the gas phase and surface chemistry processes that govern the growth of InN and indium-rich group III-nitrides alloys is of crucial importance for understanding and controlling their materials properties. *High-pressure chemical vapor deposition (HPCVD)* has been shown to be a valuable method for achieving this goal. First results show that InN layers can be grown under HPCVD conditions at 850–900 °C in the laminar flow regime of the HPCVD reactor at pressures around 15 bar and ammonia to TMI precursor flow ratio below 200. This is a major step towards the growth of indium rich group III-nitride heterostructures due to the close processing windows. The *ex situ* InN layers analysis shows that the absorption edge in the InN depends strongly on the precursor flow ratio, indicating that the debated InN properties are strongly influenced by the indium-to-nitrogen stoichiometry. By controlling the InN point defect chemistry we showed that the absorption edge shifts from 1.8 eV down to 0.7 eV. The results show a close relation between absorption edge shift in InN and In–N stoichiometry. In order to study the growth under high-pressure CVD conditions, real-time optical characterization techniques have been developed and applied to analyze gas phase constituents as well as the film nucleation and steady state growth at elevated pressures. Principal angle reflection and laser light scattering are employed to study surface chemistry processes at a sub-monolayer level, showing their superiority in optimizing and controlling the growth process.

© 2005 WILEY-VCH Verlag GmbH & Co. KGaA, Weinheim

### 1 Introduction

Improved group III-nitride materials (e.g. AlN–GaN–InN) will provide the basis for novel devices that are of significant importance due to their large spectral tunability and multi-functionality. Device structures based on  $(\text{Ga}_{1-y-x}\text{Al}_y\text{In}_x)\text{N}$  heterostructures and related alloys will for example enable the fabrication of high-efficiency, monolithic integrated energy conversion systems (multi-tandem solar cells & solid state lighting) and high speed optoelectronics for optical communication systems. At present, the growth of III-nitrides is mostly performed using low-pressure deposition techniques such as molecular beam epitaxy (MBE) [1–3] organometallic chemical vapor deposition (OMCVD – also denoted as MOVPE) [4, 5] or variations of both. However, low-pressure deposition processes are limited to regimes where the partial pressures of the constituents do not differ vastly and the decomposition process can be countered by off-equilibrium processing conditions. The application of these techniques for the growth of InN and related indium rich III-N alloys becomes a huge challenge due to their stoichiometric instabilities and low dissociation temperatures, leading to inconsistent and process dependent materials properties. Even

\* Corresponding author: e-mail: ndietz@gsu.edu

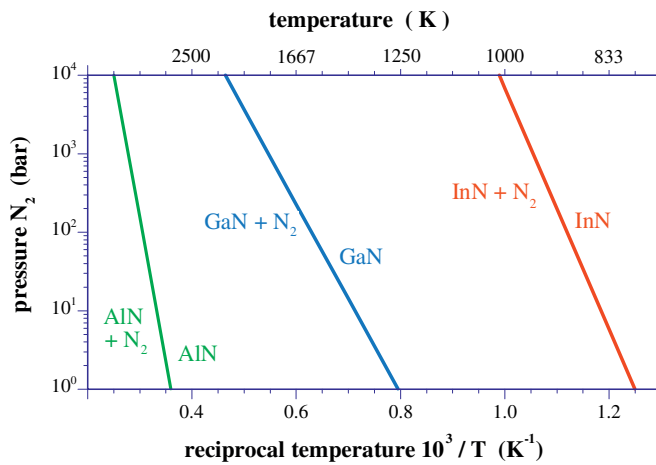


**Fig. 1** (online colour at: [www.pss-b.com](http://www.pss-b.com)) Thermal decomposition pressure vs. reciprocal temperature for AlN, GaN and InN. After MacChesney et al. [13].

for the binary InN compound itself, many of the fundamental properties are still debated. The considerable uncertainty over the band gap of InN [1, 6–8], the influence of the intrinsic materials point defect chemistry on the optical and electrical properties [9], and the effect of extrinsic impurities such as oxygen on the band gap [10, 11], show the lack of understanding in this system. Controversial reviews of the present status of InN growth and characterization were provided by Bhuiyan et al. [9] and Davydov et al. [12], implying that new approaches for the growth of In-rich group-III-nitride alloys need to be explored in order to understand and improve the structural and optical properties of InN and related alloys. Studies of the nitrogen pressure needed to prevent thermal decomposition of bulk InN provided a relationship given by

$$p(\text{N}_2) \rightarrow p_0 \exp \left[ -\frac{\Delta H_f}{R} \left( \frac{1}{T} - \frac{1}{T_0} \right) \right], \quad (1)$$

which results in the  $p - T^{-1}$  relation shown in Fig. 1 [13], where  $\Delta H_f$  represent the heat of formation,  $R$  the universal gas constant and  $T$  the equilibrium temperature. This relation indicates that in the pressure range  $p_{\text{N}_2} \leq 10^2$  bar and for substrate temperatures  $\leq 900$  K the surface decomposition of InN will be effectively suppressed. This approach was implemented at Georgia State University, leading to the first HPCVD system that allows the growth of group III-nitrides at elevated pressures. We are focusing on InN, which is the most challenging material system, since the equilibrium vapor pressure of nitrogen over InN is much higher compared to AlN and GaN [14].

## 2 HPCVD reactor

Moving towards high pressure chemical vapor deposition for the growth of group III-nitrides, required a completely new reactor system design, with additional considerations towards flow kinetics, gas phase reactions, diffusion through the surface boundary layer as well as altered surface chemistry. A high-pressure flow channel reactor was constructed, where the flow channel is embedded in the inner reactor cylinder, while an outer reactor confines the overall pressure of the reactor to well above 100 bar. A symmetric arrangement of substrates in the upper and lower part of the flow channel is used to prevent preferential material deposition. As schematically depicted in Fig. 2, optical access ports are integrated at the center axis of the substrates, allowing the optical characterization of flow kinetics, gas phase reactions and the substrate surface from the back side through the substrate. At above atmospheric pressures, optical diagnostic techniques are uniquely suited to provide real time information pertaining to gas flow dynamics in both laminar and turbulent flow regimes. Optical diagnostic techniques were utilized to obtain crucial information pertaining to the precursor flow and their decomposition kinetics. Several

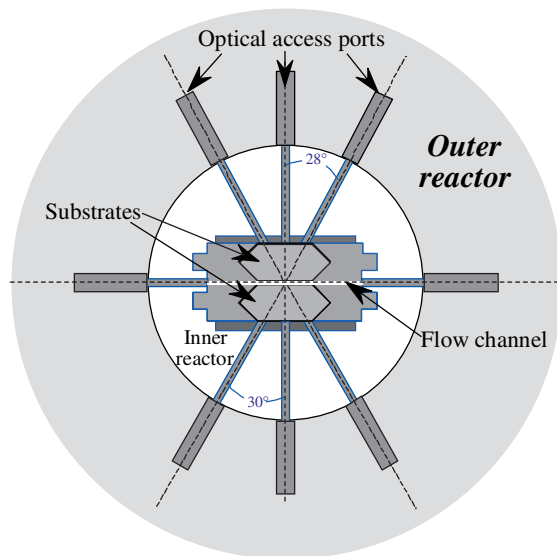


**Fig. 2** (online colour at: [www.pss-b.com](http://www.pss-b.com)) Schematic cross section of the reactor containing the optical access ports and the center of the substrates. Two optical ports provide access to the flow channel and three ports in each of the two half sections of the reactor provide access to the growth surface.

optical techniques have been explored, but only a small group satisfies the requirements of being robust as well as sensitive. For example, the substrate temperature during typical InN growth is between 800 K and 1100 K, emitting significant radiation. The radiation emitted from the heated substrate limits the sensitivity of many optical probe techniques in the visible and infra-red (IR) regime, even if modulation techniques are applied. However, the radiation intensity for a 1000 K back body emitter below 350 nm vanishes quickly with negligible contributions below 300 nm. This allows the utilization of ultraviolet absorption spectroscopic (UVAS) techniques to identify the group-V and organometallic group-III precursors in the gas phase [15–18]. A more detailed description of the reactor design and the optical characterization capabilities is given elsewhere [19–23].

The integration of optical monitoring capabilities for gas flow, gas phase decomposition kinetics, as well as surface reactions is crucial to gain insights in the growth process and in order to control the process on a sub-monolayer level in real-time. In addition, the growth of InN at high pressures requires serious attention towards *minimization* of gas phase reactions, extracting sufficient organometallic (OM) nutrients from the OM-bubblers, and embedding the precursor flows in the reactor main stream. Those considerations led to the design of a pulsed precursor injection scheme, which is essential for

- compression of precursors to reactor pressure,
- minimization of gas phase reactions,
- engineered nucleation kinetics and layer growth, and
- analyzing the gas-phase and surface decomposition dynamics in real-time.

### 3 Real-time optical monitoring and reactor flow characterization

Real-time monitoring capabilities were used to analyze the flow characteristics in the HPCVD reactor using laser light scattering (LLS) in forward scattering geometry [24]. The onset of increased LLS indicating the flow and pressure regime at which laminar flow can be maintained. The associated Reynolds number averaged around 1480 with no significant pressure dependency [25]. For the precursor injection in the HPCVD reactor, a two step process has been chosen: In the first step, a reservoir is filled at slightly above atmospheric pressure, which in the second step is compressed with carrier gas to the reactor pressure and temporally controlled injected into the reactor. The repetition rate, duration of injection, as well as the position of injection within a given cycle sequence are process parameter that are used to control gas phase reactions and the growth process itself. The influence of pressure and flow on such precursor pulses traveling through the reactor is illustrated in Fig. 3 as an example of TMI [In(CH<sub>3</sub>)<sub>3</sub>]

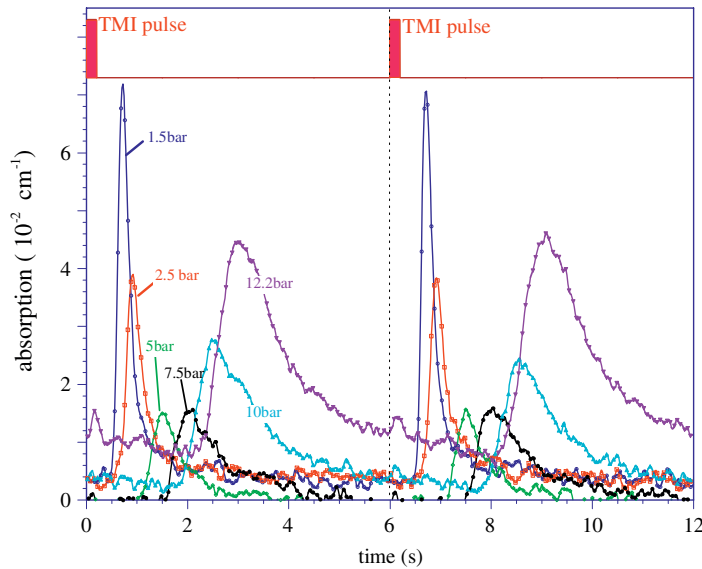


**Fig. 3** (online colour at: www.pss-b.com) Absorption traces monitored at 210.7 nm during TMI precursor pulse injection in the reactor at constant flow of 5 slm. The reactor pressure was varied between 1 and 12 bar. The pulse cycle sequence is 6 s with 0.2 s TMI injection time.

pulses injected with a sequence repetition rate of 6 sec. As the pressure in the reactor increases, the TMI pulses monitored at the substrate center line show three distinct features:

- a systematic shift in the pulse arrival time,
- a systematic TMI pulse broadening, and
- an initial decrease of the absorption peak maximum with an increase as the pressure further increases.

The systematic shift in the pulse arrival time can be analyzed in terms of a reactor specific geometry constant, the reactor pressure  $p_r$  (in bar) and the gas flow  $V_{slm}$  through the reactor. The analysis allowed the computation of the average gas velocity  $v_g$  in the reactor system given by

$$v_g = 136.7 \cdot \frac{V_{slm}}{p_r}, \quad (2)$$

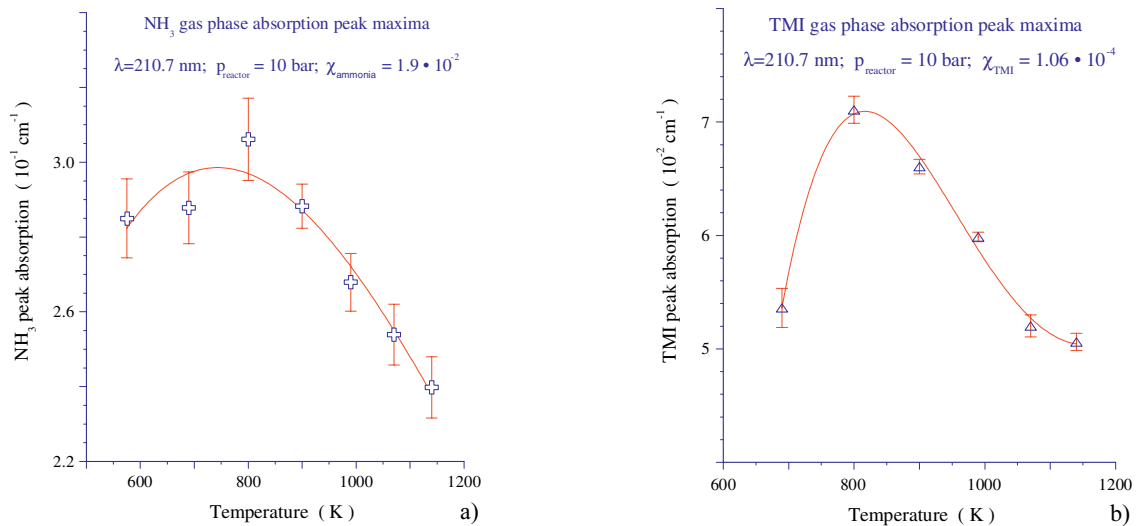


**Fig. 4** (online colour at: www.pss-b.com) a) Change of the ammonia absorption peak maximum as function of temperature. b) Decomposition of TMI at 10 bar reactor pressure, monitored during pulsed TMI injection as function of temperature.

providing an analysis of the gas flow kinetics with the possibility to precisely engineer the pulse shape and precursor overlaps during the growth of group III-nitride compounds.

The decomposition dynamics of the precursors were analyzed in the temperature regime of 300 K to 1200 K. Figure 4a shows the temperature dependant ammonia  $[\text{NH}_3]$  absorption monitored at 210.7 nm for a reactor pressure of 10 bar. The decomposition at 10 bar pressure starts at approx. 850 K, which is significantly reduced as compared to the decomposition temperature under atmospheric pressure, where the onset of ammonia decomposition is observed at approx. 990 K [22]. The decomposition dynamics for TMI is depicted in Fig. 4b, showing that the onset of decomposition in the gas phase occurs around 800 K, slightly higher than those reported under low-pressure OMCVD conditions [16, 26] for the growth of In-group V compounds [27, 28].

The observed decrease in the ammonia decomposition temperature with increase of reactor pressure is very crucial for InN growth optimization and the control of the point defect chemistry in this material system. It also allows to make more efficient use of the ammonia precursor, enabling a lower ammonia to TMI flow ratio.

#### 4 Real-time optical characterization of InN growth

The decomposition studies for ammonia in the previous section suggest temperatures well above 900 K are needed for sufficient cracking of the ammonia precursor for the growth of InN. However, literature data for InN growth by OMCVD indicate a growth temperature of 675 K to 750 K [5], 775 K [29], 810 K–840 K [30]. Under HPCVD conditions, it is possible to increase the growth temperature about 50 K–150 K higher than possible under low-pressure OMCVD conditions [21, 31]. However, this may still leave a temperature mismatch between optimum ammonia decomposition and optimal InN growth temperature. The observed onset of ammonia decomposition temperature decreases with increasing reactor pressure, which is a significant advantage as compared to low-pressure OMCVD, where TMI: $\text{NH}_3$  ratios of  $1:10^4$  and larger [5, 29] are required to counteract the low ammonia decomposition rate at optimum growth temperatures.

The HPCVD system allows the exploration of a large parameter space for the evaluation of the optimum growth conditions, such as

- reactor pressure  $p$ ,
- average gas velocity  $v_g$ ,
- TMI and ammonia pulse separation and reaction time,
- the molar ratio TMI to ammonia, and
- growth temperature.

This large parameter space inevitably requires the application of real-time optical monitoring to assess the nucleation and growth conditions and to optimize the growth of InN and related materials. For monitoring InN nucleation and growth, gas phase UV absorption spectroscopy, single wavelength principal angle reflectance (PAR) [19, 32] and laser light scattering (LLS) are applied simultaneously. PAR is based on the same principle as  $p$ -polarized reflectance spectroscopy [32, 33]. However, PAR utilizes  $p$ -polarized light impinging the substrate–ambient interface near the principal angle  $\varphi_p$ , corresponding to the pseudo-Brewster angle  $\varphi_B$  for  $p$ -polarized light impinging the ambient–substrate interface [19]. The angle of total reflection,  $\varphi_T$ , is approximately 5 deg above  $\varphi_p$ .

Figure 5 shows the PAR trace recorded for the wavelength  $\lambda = 6328 \text{ \AA}$ , during InN growth under HCVD conditions. Superimposed on the interference oscillations is a fine structure that is strongly correlated to the time sequence of the supply of precursors employed. Each peak in the fine structure corresponds to a complete precursor cycle sequence. The LLS trace indicates that the surface roughness during growth remains low and even slightly decreases. An *ex situ* analysis of the optical properties is given further below.

The fine structure, superimposed on the PARS trace, is shown in more detail in the top trace in Fig. 6a and b for the InN nucleation stage and under steady state growth conditions, respectively. The lower half shows the UV absorption traces recorded for the wavelength  $\lambda = 210.8 \text{ nm}$ , monitoring the un-decom-

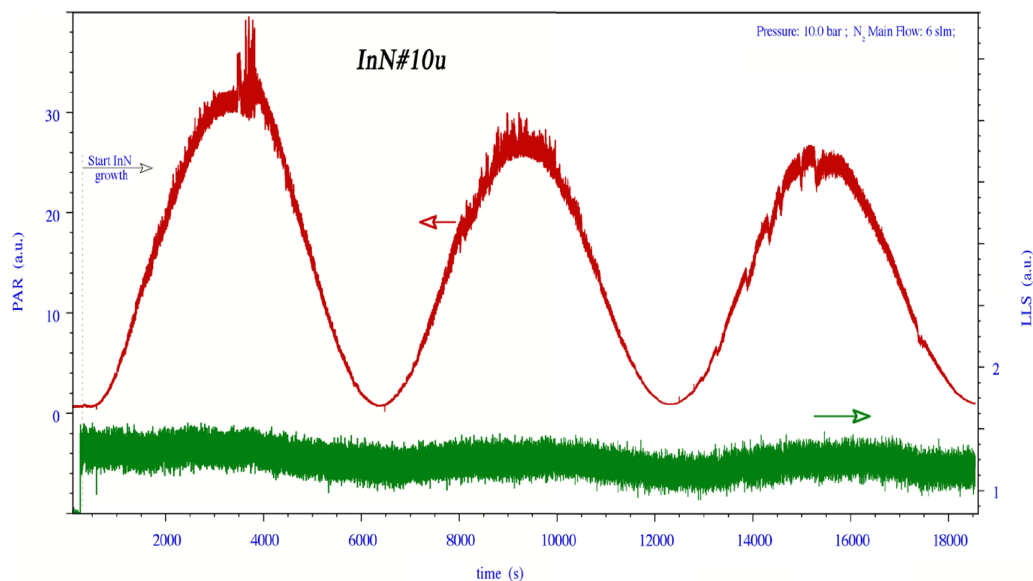


Fig. 5 (online colour at: www.pss-b.com) Real-time optical monitoring of InN growth by PAR and LLS.

posed ammonia and TMI species above the growth surface. The PAR trace in the upper half of the figure is recorded for the wavelength  $\lambda = 6328 \text{ \AA}$ , monitoring highly sensitive changes in the dielectric function at the substrate-ambient interface. Also indicated in the figure are the positions of the precursor pulse injections with a total cycle sequence repetition time of 6 sec. Note that here is a distinct time-lag between precursor pulse position (opening of valve) and the corresponding optical response. The time lag (see arrows) relates to the average gas velocity and the travel distance between the valve and the monitoring point [22]. As depicted in Fig. 6a, it takes about one to two cycle sequences before the UV absorption feature for TMI clearly can be observed (see arrows). The PAR signal shows a large increase after the ammonia pulse reaches the substrate, indicating the start of nucleation on InN and the presence of TMI fragments in the surface vicinity. The UV gas phase absorption is monitored simultaneously with

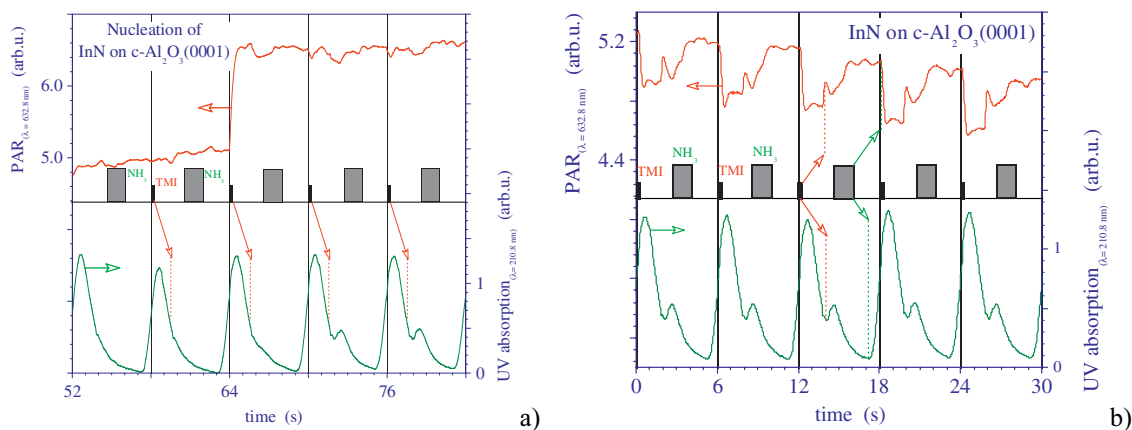


Fig. 6 (online colour at: www.pss-b.com) a) Top trace: principal angle reflectance (PAR) fine structure oscillation monitored during InN nucleation. Bottom trace: UVAS trace monitored at 201.8 nm. A precursor cycle sequence of 6 sec with 0.4 sec TMI and 1.4 sec ammonia pulses, separated by 1.4 sec were used. b) PAR and UV absorption traces during steady-state InN growth at 990 K. The reactor pressure was 10 bar with a total flow of 5 slm. The overall decrease in the PAR signal corresponds to average InN growth.

the PARS signal as depicted in the lower part of Fig. 6a. The UV gas phase absorption trace monitors the undecomposed concentration of both precursors, TMI and ammonia, in the gas phase above the growth surface [23]. Both the UVAS and PARS trace provide a snapshot of the growth conditions at the center axis of the substrate.

A steady-state surface chemistry is typically reached after 5 to 20 cyclic precursor exposures, depending on substrate temperature, precursor flow ratio, gas phase velocity and reactor pressure. Figure 6b shows the PAR and UVAS responses during steady-state growth conditions. The periodic modulation of the PAR response can be directly correlated to the presence of ammonia and TMI fragments in a surface reaction layer and at the growth surface. The overall decrease in the PAR signal is correlated to the InN growth per cycle sequence as discussed in detail for *p*-polarized reflectance [32, 33]. Note that the variation of the process parameters/conditions along the flow direction are not accessible and will require comprehensive flow and reactor modeling. Such a process model will have to include details on the temporal fine structure evolution and the correlation to gas phase constituents as obtained by UVAS which is discussed in earlier publications [32]. PARS is a highly sensitive surface diagnostic tool with sub-monolayer resolution, able to operate at high pressures, illustrated in Fig. 6. Its surface sensitivity enables the tracking of variations in surface constituents, which can be linked to the evolution of precursor species/fragments in the gas phase. The results of the decomposition dynamics provide the initial basis for a more detailed understanding of the dissociation of the precursors ammonia and TMI and of the reaction rate constants for growth of InN as theoretical predicted by Cardelino et al. [31]. The real-time diagnostic tools employed are uniquely suited to follow the growth process with sub-monolayer resolution and to engineer/control the layer quality/properties of indium rich group III-nitrides.

## 5 Ex-situ InN layer characterization

The structural properties of epitaxially grown InN films have been investigated using X-ray diffraction. Figure 7 depicts the XRD spectra recorded in the  $\omega$ - $2\theta$  mode for characteristic samples #22U, #24L\_A and #25L\_C where the precursor flow ratio  $R_{\text{NH}_3:\text{TMI}}$  was systematic lowered from 8000 down to 200. The growth temperature was 850 °C, with a reactor pressure of 11 bar and an average gas flow velocity of 45 cm/s. Sample #22U shows a broad reflection from wurtzite-type InN centered at 31.26 deg with full-width at half-maximum (FWHM) of 650 arcsec. The structural layer quality is equivalent to MBE grown InN layer grown on a GaN/AlN buffer layers on sapphire [34]. In sample #24L\_A, the precursor flow ratio  $R_{\text{NH}_3:\text{TMI}}$  is lowered to 1000. Under these conditions the InN (002) reflection is broadened and shifted to 31.2° and the InN (101) reflection at 31.1° becomes more pronounced. For a  $R_{\text{NH}_3:\text{TMI}}$  around 200 (sample #25L\_C), both InN (002) and InN (101) reflection show distinct double structures, indicating the existence of phases with FWHM's below 200 arcsec in very close proximity. The analysis of the

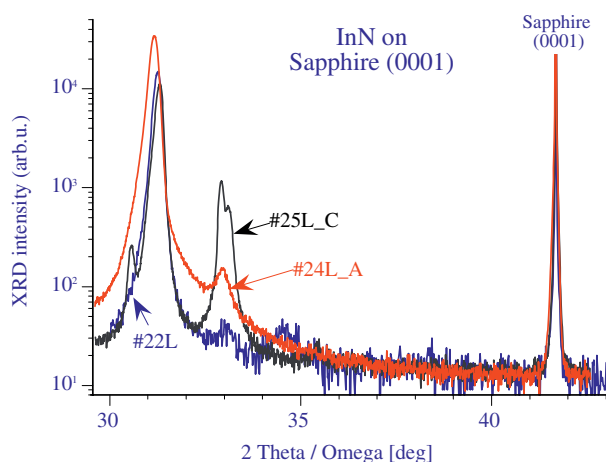


**Fig. 7** (online colour at: [www.pss-b.com](http://www.pss-b.com)) XRD spectra from InN layers grown with precursor flow ratio  $R_{\text{NH}_3:\text{TMI}}$  of 8000 (#22L), 1000 (#24L\_A) and 200 (#25L\_C).

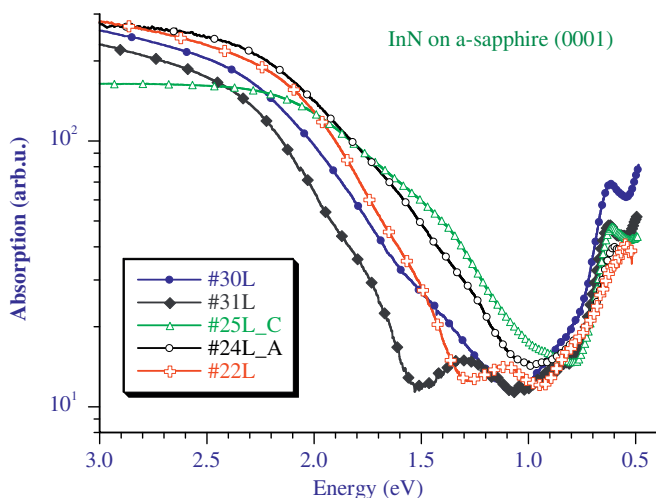


**Fig. 8** (online colour at: [www.pss-b.com](http://www.pss-b.com)) Shift of absorption edge for five characteristic InN samples grown with different ammonia to TMI ratio.

X-ray spectra on (102) and (002) reflection planes for the samples #22U and #25L\_C provided the lattice constants  $a = 3.557 \text{ \AA}$  and  $c = 5.754 \text{ \AA}$ . These values are quite close to the other reported values of  $a = 3.548 \text{ \AA}$  and  $c = 5.76 \text{ \AA}$  of Tansley et al. [35],  $a = 3.544 \text{ \AA}$  and  $c = 5.718 \text{ \AA}$  of Osamura et al. [36], and  $c = 5.69 \text{ \AA}$  of Wakahara et al. [37]

At this point, it can not be excluded that the observed asymmetric line shapes for the InN (002) and InN (101) reflections are caused due to the close proximity of Indium oxide ( $\text{In}_2\text{O}_3$ ) reflections, which are reported at  $30.58^\circ$  for  $\text{In}_2\text{O}_3$  (222),  $33.09^\circ$  for  $\text{In}_2\text{O}_3$  (321), and  $35.54^\circ$  for  $\text{In}_2\text{O}_3$  (400) [38]. The appearance of additional distinct sharp reflections as seen in sample #25L\_C does not match known Indium oxide ( $\text{In}_2\text{O}_3$ ) peak positions.

Figure 8 shows the absorption spectra observed for a set of characteristic samples #22L, #24L\_A, #25L\_C, #30L and #31L. Samples #30L and #31L are grown with a  $R_{\text{NH}_3:\text{TMI}}$  ratio of 450 and a substrate temperature of  $850 \text{ }^\circ\text{C}$ . The reactor pressure was 15 bar with a gas flow velocity of  $50 \text{ cm/s}$ . As depicted in Fig. 8, all samples show a dominant absorption structure centered at  $0.63 \text{ eV}$ . For estimated high  $R_{\text{NH}_3:\text{TMI}}$  precursor ratios (#31L  $\rightarrow$  #30L  $\rightarrow$  #22L) the absorption edge shifts downwards from an estimated  $1.5 \text{ eV}$  to approximate  $1.0 \text{ eV}$ , with absorption peaks / shoulders at  $0.87 \text{ eV}$ ,  $1.1 \text{ eV}$  and  $1.3 \text{ eV}$ . For sample #24L\_A the absorption edge is shifted below  $0.9 \text{ eV}$  and sample #25L\_C suggest already an overall shifted absorption edge around  $0.7 \text{ eV}$ . The absorption peak centered at  $0.63$  remains in its strength and position. It has been assigned to plasmon excitations in the conduction band [39] due to large free carrier concentration. If this theory holds, it would suggest that the absorption edge shift towards lower energies is not directly related to the free carrier concentration, but rather to stoichiometry variations in InN [40].

The development of the absorption structures for these five samples suggest that the observed absorption edge shift from  $1.5 \text{ eV}$  down to below  $0.7 \text{ eV}$  is caused by a series of absorption structures, centered around  $1.3 \text{ eV}$ ,  $1.1 \text{ eV}$ , and  $0.87 \text{ eV}$ . The appearance and strength of these absorption centers correlate/coincide with the reduction of the ammonia to TMI precursor flow ratio, suggesting a close correlation between precursor ratio and the stoichiometry of the deposited layers.

## 6 Conclusion

For the growth of InN and related materials we introduced the first high-pressure CVD reactor capable of operating at pressures of up to 100 bar. The growth of InN has been explored in the laminar flow regime, evaluating the growth parameter for reactor pressures in range of 10 to 15 bars, gas flow velocities from  $20$  to  $50 \text{ cm s}^{-1}$ , and molar ammonia to TMI ratios between 200 to 8000. High quality InN layers were achieved for growth temperatures in the range of  $830 \text{ }^\circ\text{C}$  to  $850 \text{ }^\circ\text{C}$ .

For the real-time optical growth characterization, we introduced principle angle reflectance spectroscopy (PARS) and demonstrated that PARS and LLS are able to follow the film growth process with sub-monolayer resolution, which will be an important tool for engineered nano-scale device structures. The link between the surface sensitive PARS response to the real-time gas phase analysis (UVAS) allows to establish a comprehensive growth/flow model that will provide crucial insights in the gas phase decomposition kinetics, surface chemistry processes, and the film growth process at high pressures. Such a reactor model will be essential for the exploration of high-pressure process parameters that lead to turbulent flow conditions.

The optical InN layer characterization results indicate that the shift of the absorption edge from 1.8 eV down to approximate 0.7 eV is closely related to the precursor flow ratio and with it to stoichiometry of the InN layer. The initial results suggest that the optimum molar flow ratio, ammonia to TMI, under HPCVD conditions is below 200, which is due to the efficient cracking of the nitrogen precursor at the high reactor pressure and high growth temperature. Further studies varying the ammonia to TMI flow ratio, the center flow velocity, and the growth temperatures will be needed to assess the optimum growth window. The initial results demonstrate that the high-pressure CVD approach produces InN layer of equivalent quality to MBE grown InN layer. The good match to the GaN and AlN growth windows will enable the exploration of indium rich  $\text{In}_{1-x}\text{Ga}_x\text{N}$  and  $\text{In}_{1-x}\text{Al}_x\text{N}$  alloys and heterostructures. Even higher processing temperatures might be possible by further increasing the reactor pressure.

**Acknowledgements** This work was supported by NASA grant NAG8-1686 and GSU-RPE. M.S. gratefully acknowledges the fellowship of the Alexander von Humboldt-foundation.

## References

- [1] T. Inushima, V. V. Mamutin, V. A. Vekshin, S. V. Ivanov, T. Sakon, M. Motokawa, and S. Ohoya, *J. Cryst. Growth* **227/228**, 481–485 (2001).
- [2] J. Wu, W. Walukiewicz, W. Shan, K. M. Yu, J. W. Ager III, E. E. Haller, Hai Lu, and W. J. Schaff, *Phys. Rev. B* **66**(11), 201403 (2002).
- [3] R. A. Oliver, C. Nörenberg, M. G. Martin, M. R. Castell, L. Allers, and G. A. D. Briggs, *Surf. Sci.* **532–535**, 806–810 (2003).
- [4] J. Aderhold, V. Yu. Davydov, F. Fedler, H. Klausning, D. Mistele, T. Rotter, O. Semchinova, J. Stemmer, and J. Graul, *J. Cryst. Growth* **222**(4), 701–705 (2001).
- [5] Z. X. Bi, R. Zhang, Z. L. Xie, X. Q. Xiu, Y. D. Ye, B. Liu, S. L. Gu, B. Shen, Y. Shi, and Y. D. Zheng, *Mater. Lett.* **58**(27/28), 3641–3644 (2004).
- [6] J. Wu, W. Walukiewicz, K. M. Yu, J. W. Ager III, E. E. Haller, H. Lu, W. J. Schaff, Y. Saito, and Y. Nanishi, *Appl. Phys. Lett.* **80**(21), 3967–3969 (2002).
- [7] I. Vurgaftman and J. R. Meyer, *J. Appl. Phys.* **94**, 3675–3696 (2003).
- [8] V. Yu. Davydov and A. A. Klochikhin, *Semiconductors* **38**(8), 861–898 (2004).
- [9] A. G. Bhuiyan, A. Hashimoto, and A. Yamamoto, *J. Appl. Phys.* **94**(5), 2779–2808 (2003).
- [10] E. Kurimoto, M. Hangyo, H. Harima, M. Yoshimoto, T. Yamaguchi, T. Araki, Y. Nanishi, and K. Kisoda, *Appl. Phys. Lett.* **84**(2), 212–214 (2004).
- [11] K. S. A. Butcher, M. Wintrebert-Fouquet, P. P.-T. Chen, T. L. Tansley, H. Dou, S. K. Shrestha, H. Timmers, M. Kuball, K. E. Prince, and J. E. Bradby, *J. Appl. Phys.* **95**(11), 6124–6128 (2004).
- [12] V. Yu. Davydov, A. A. Klochikhin, V. V. Emtsev, A. V. Sakharov, S. V. Ivanov, V. A. Vekshin, F. Bechstedt, J. Furthmüller, J. Aderhold, J. Graul, A. V. Mudryi, H. Harima, A. Hashimoto, A. Yamamoto, J. Wu, H. Feick and E. E. Haller, *Proc. SPIE* **5023**, 68–71 (2003).
- [13] J. MacChesney, P. M. Bridenbaugh, and P. B. O'Connor, *Mater. Res. Bull.* **5**, 783–792 (1970).
- [14] O. Ambacher, M. S. Brandt, R. Dimitrov, T. Metzger, M. Stutzmann, R. A. Fischer, A. Miehr, A. Bergmayer, and G. Dollinger, *J. Vac. Sci. Technol. B* **14**(6), 3532–3542 (1996).
- [15] G. A. Hebner, K. P. Killeen, and R. M. Biefeld, *J. Cryst. Growth* **98**(3), 293–301 (1989).
- [16] G. A. Hebner and K. P. Killeen, *J. Appl. Phys.* **67**(3), 1598–1600 (1990).
- [17] H. Okabe, M. K. Emadi-Babaki, and V. R. McCrary, *J. Appl. Phys.* **69**(3), 1730–1735 (1991).
- [18] M. C. Johnson, K. Poochinda, N. L. Ricker, J. W. Rogers, Jr., and T. P. Pearsall, *J. Cryst. Growth* **212**(1/2), 11–20 (2000).

- [19] N. Dietz, S. McCall, and K. J. Bachmann, Proc. Microgravity Conf. 2000, NASA/CP-2001-210827, pp. 176–181 (2001).
- [20] N. Dietz, V. Woods, S. McCall, and K. J. Bachmann, Proc. Microgravity Conf. 2002, NASA/CP-2003-212339, pp. 169–181 (2003).
- [21] B. H. Cardelino, C. E. Moore, S. D. McCall, C. A. Cardelino, N. Dietz, and K. J. Bachmann, CAITA-2004, Purdue University, June 2004, ISBN 86-7466-117-3 (2004).
- [22] N. Dietz, M. Strassburg, and V. Woods, J. Vac. Sci. Technol. A **23**(4), 1221–1227 (2005).
- [23] N. Dietz, Indium-nitride growth by HPCVD: Real-time and ex-situ characterization, book chapter in: GaN-based Materials: Epitaxy and Characterization, edited by Z. C. Feng (Imperial College Press (ICP), 2005), pp. 1–31.
- [24] V. Woods, H. Born, M. Strassburg, and N. Dietz, J. Vac. Sci. Technol. A **22**(4), 1596–1599 (2004).
- [25] V. Woods and N. Dietz, Mater. Sci. Eng. B (2005), accepted.
- [26] J. Haigh and S. O'Brien, J. Cryst. Growth **68**, 550–556 (1984).
- [27] N. I. Buchan, C. A. Larsen, and G. B. Stringfellow, J. Cryst. Growth **92**, 591–604 (1988).
- [28] R. J. S. J. A. McCaulley and V. M. Donnelly, J. Vac. Sci. Technol. A **9**(6), 2872–2886 (1991).
- [29] T. Schmidling, M. Drago, U. W. Pohl, and W. Richter, J. Cryst. Growth **248**, 523–527 (2003).
- [30] A. Jain, S. Raghavan, and J. M. Redwing, J. Cryst. Growth **269**(1), 128–133 (2004).
- [31] B. H. Cardelino, C. E. Moore, C. A. Cardelino, S. D. McCall, D. O. Frazier, and K. J. Bachmann, J. Phys. Chem. A **107**(19), 3708–3718 (2003).
- [32] N. Dietz, Mater. Sci. Eng. B **87**(1), 1–22 (2001).
- [33] N. Dietz and K. J. Bachmann, Vacuum **47**, 133–140 (1996).
- [34] K. M. Yu, Z. Liliental-Weber, W. Walukiewicz, W. Shan, J. W. Ager, III, S. X. Li, R. E. Jones, E. E. Haller, Hai Lu, and William J. Schaff, Appl. Phys. Lett. **86**, 071910 (2005).
- [35] T. L. Tansley and C. P. Foley, J. Appl. Phys. **59**(9), 3241–3244 (1986).
- [36] K. Osamura, S. Naka, and Y. Murakami, J. Appl. Phys. **46**(8), 3432–3437 (1975).
- [37] Akihiro Wakahara and Akira Yoshida, Appl. Phys. Lett. **54**(8), 709–711 (1989).
- [38] JCPDS International Centre for Diffraction Data, file No. 76-0152.
- [39] D. B. Haddad, J. S. Thakur, V. M. Naik, G. W. Auner, R. Naik, and L. E. Wenger, Mater. Res. Soc. Symp. Proc. **743**, L11.22 (2003).
- [40] K. Scott, A. Butcher, M. Wintrebert-Fouquet, P. P.-T. Chen, K. E. Prince, H. Timmers, S. K. Shrestha, T. V. Shubina, S. V. Ivanov, R. Wuhrer, M. R. Phillips, and B. Monemar, phys. stat. sol. (c) **2**(7), 2263–2266 (2005).